Author Manuscript

Author Manuscript

Author Manuscript

Author Manuscript

HHS Public Access

Author manuscript

Neuron. Author manuscript; available in PMC 2017 July 26.

Published in final edited form as:

Neuron. 2016 July 20; 91(2): 412–424. doi:10.1016/j.neuron.2016.06.010.

Activation of direct and indirect pathway medium spiny neurons drives distinct brain-wide responses

Hyun Joo Lee[1,†], **Andrew J. Weitz**[1,2,†], **David Bernal-Casas**[1], **Ben A. Duffy**[1], **ManKin Choy**[1], **Alexxai V. Kravitz**[3,4], **Anatol C. Kreitzer**[4], and **Jin Hyung Lee**[1,2,5,6,*]

[1]Department of Neurology and Neurological Sciences, Stanford University, Stanford, CA 94305, USA

[2]Department of Bioengineering, Stanford University, Stanford, CA 94305, USA

[3]National Institute of Diabetes and Digestive and Kidney Diseases, National Institute of Health, Bethesda, MD 20892, USA

[4]Gladstone Institute of Neurological Disease, University of California, San Francisco, CA 94158, USA

[5]Department of Neurosurgery, Stanford University, Stanford, CA 94305, USA

[6]Department of Electrical Engineering, Stanford University, Stanford, CA 94305, USA

Summary

A central theory of basal ganglia function is that striatal neurons expressing the D1 and D2 dopamine receptors exert opposing brain-wide influences. However, the causal influence of each population has never been measured at the whole-brain scale. Here, we selectively stimulated D1 or D2 receptor-expressing neurons while visualizing whole-brain activity with fMRI. Excitation of either inhibitory population evoked robust positive BOLD signals within striatum, while downstream regions exhibited significantly different and generally opposing responses consistent with – though not easily predicted from – contemporary models of basal ganglia function. Importantly, positive and negative signals within the striatum, thalamus, GPi, and STN were all associated with increases and decreases in single-unit activity, respectively. These findings provide direct evidence for the opposing influence of D1 and D2 receptor-expressing striatal neurons on brain-wide circuitry and extend the interpretability of fMRI studies by defining cell type-specific contributions to the BOLD signal.

[*]Correspondence to: Jin Hyung Lee, PhD ljinhy@stanford.edu 1201 Welch Road, #P206 Stanford, CA 94305.
[†]These authors contributed equally

Author contributions: HJL performed surgeries, behavioral tests, ofMRI experiments, and electrophysiology. AJW analyzed ofMRI data, made figures, and wrote the paper. DBC analyzed electrophysiology data. BAD reconstructed ofMRI data. MKC analyzed behavioral data and performed immunohistochemistry. AVK and ACK helped with the animal model, surgery, and electrophysiology during early phases of the experiments. JHL planned the study, analyzed and interpreted all data, wrote the paper, and supervised all aspects of the study.

Author Manuscript Author Manuscript Author Manuscript Author Manuscript

Introduction

Medium spiny neurons (MSNs) make up as much as 95% of cells within the striatum and send inhibitory projections to surrounding nuclei of the basal ganglia (Gerfen, 2004; Kemp and Powell, 1971). According to the model of basal ganglia circuit function first established by Albin and DeLong (Albin et al., 1989; DeLong, 1990), MSNs facilitate and suppress motor behavior via the direct and indirect pathways, respectively. The direct pathway promotes motor behavior by actively inhibiting the basal ganglia's two GABAergic output nuclei – the internal globus pallidus (GPi) and substantia nigra pars reticulata (SNr) – which in turn project to thalamocortical and brainstem motor circuits. The reduction in inhibitory signals leaving the basal ganglia results in disinhibition of these circuits, allowing them to execute the commands necessary for movement. In contrast, the indirect pathway, which includes additional synapses onto the external globus pallidus (GPe) and subthalamic nucleus (STN), increases the activity of the basal ganglia's output nuclei. This increase in activity results in suppression of thalamocortical circuitry and ultimately inhibits movement. While this feedforward description of the basal ganglia can account for much of its behavior in normal and pathological conditions, the existence of additional connections in the form of collateral branching, reciprocal connectivity, recurrent networks, and feedback loops suggests much greater complexity. These include collaterals from D1 receptor-expressing MSNs to GPe (Cazorla et al., 2014; Matamales et al., 2009), reciprocal connections along the striato-GPe-STN axis (Miwa et al., 2001), the "hyperdirect" pathway from cortex to STN (Monakow et al., 1978; Nambu et al., 2002), intranigral inhibitory connections (Mailly et al., 2003), as well as other projections from thalamus to striatum (Smith et al., 2004) and from GPe to cortex (Saunders et al., 2015). Thus, while the feedforward view of direct and indirect pathways remains a powerful holistic tool, the exact influence of D1- and D2-MSNs remains difficult to predict at the whole-brain scale.

Historically, it has been difficult to disentangle the functional properties of striatal MSNs belonging to the direct or indirect pathway, because they are highly anatomically intermingled. However, the MSNs that constitute each pathway also share relatively distinct neurochemical identities. MSNs of the direct pathway primarily express the D1 dopamine receptor (D1-MSNs), while those of the indirect pathway primarily express the D2 dopamine receptor (D2-MSNs) (Deng et al., 2006; Gerfen et al., 1990). Advances in molecular biology and genetic engineering have thus made it possible to selectively express transgenes, including optogenetic tools, in each population (Cui et al., 2013; Gong et al., 2007; Kravitz et al., 2010; Kravitz et al., 2012; Lobo et al., 2010). Several studies have exploited this ability in order to selectively excite each population in isolation and measure downstream effects on behavior and firing rates using *in vivo* electrophysiology. For example, it has been shown that direct pathway stimulation reduces hypokinetic behavioral deficits, while indirect pathway stimulation exacerbates them (Kravitz et al., 2010). Similarly, inhibition and excitation of SNr neurons evoked by D1- or D2-MSN stimulation have been shown to correlate with motor facilitation and suppression, respectively (Freeze et al., 2013). Finally, activation of direct and indirect pathway MSNs evoked and suppressed activity in motor cortex, respectively, although non-opposing effects were also observed in a subset of neurons (Oldenburg and Sabatini, 2015). These findings support the prevailing

Author Manuscript Author Manuscript Author Manuscript Author Manuscript

view of basal ganglia circuit function that the direct and indirect pathways selectively turn on or off the thalamocortical loop. Yet direct evidence for these two pathways' differential effect on macroscopic circuit function remains lacking. Here, we combined targeted optogenetic stimulation of the direct and indirect pathways with functional MRI to reveal the causal influence of each population on activity across the whole brain including areas within the basal ganglia, thalamus, and cortex. This integration of optogenetic stimulation with fMRI (termed ofMRI) has enabled the causal influence of genetically defined neuronal populations on downstream regions to be measured directly (Abe et al., 2012; Desai et al., 2011; Duffy et al., 2015; Gerits et al., 2012; Kahn et al., 2013; Lee et al., 2010; Liu et al., 2015; Ohayon et al., 2013; Weitz et al., 2015; Weitz and Lee, 2013).

Results

Optogenetic targeting of direct and indirect pathways

To selectively activate D1- or D2-MSNs *in vivo*, we used BAC transgenic mouse lines expressing Cre-recombinase under control of D1 or D2 dopamine receptor regulatory elements (Cui et al., 2013; Gong et al., 2007; Kravitz et al., 2010; Kravitz et al., 2012; Lobo et al., 2010). A double-floxed inverted recombinant AAV1 virus was injected into dorsomedial striatum to express the excitatory opsin ChR2-EYFP in Cre-positive D1- or D2-MSNs and enable selective optogenetic control of the direct or indirect pathway, respectively. Histological examination confirmed that ChR2-EYFP was localized to MSNs in the striatum, with over 87% of ChR2-EYFP+ cells co-expressing the MSN marker DARPP32 in both D1-Cre (Figure 1A,B) and D2-Cre mice (Figure 1E,F). This percentage is consistent with previous reports of AAV1-mediated ChR2 expression in D1 and D2 BAC transgenic lines (Kravitz et al., 2010). To demonstrate specificity for each pathway, we also quantified neuronal co-expression of the D1 marker prodynorphin and the D2 marker enkephalin. In D1-Cre mice, 89% of ChR2-EYFP+ cells co-expressed prodynorphin (Figure 1A,B), while in D2-Cre mice, 83% of ChR2-EYFP+ cells co-expressed enkephalin (Figure 1E,F). ChR2 expression was thus well restricted to the targeted populations.

In vivo activation was enabled by stereotactic implantation of a fiber-optic cannula at the dorsomedial striatum. Pulse trains were delivered for 20 s (15 ms pulse width at 2.5 mW and 20 Hz frequency) since this temporal paradigm has previously been shown to evoke robust BOLD signals both locally and remotely (Duffy et al., 2015; Lee et al., 2010; Liu et al., 2015; Weitz et al., 2015), as well drive behavioral changes during D1- and D2-MSN stimulations (Kravitz et al., 2010). Before fMRI experiments, the motor behavior of freely moving animals was monitored during 20 s periods of stimulation. These experiments served to confirm both that light delivery could elicit a behavioral response and that stimulation was sufficiently restricted to MSNs of the direct or indirect pathway. As shown previously (Kravitz et al., 2010), unilateral stimulation of D1-MSNs elicited a significant increase in contraversive rotations (Figure 1C; $p = 0.0003$, two-tailed paired t-test), while stimulation of D2-MSNs elicited a significant increase in ipsiversive rotations (Figure 1G; $p = 0.002$). Contraversive rotations also significantly decreased during D2-MSN stimulation (Figure 1G; $p = 0.006$). These behavioral effects are consistent with the classical model of basal ganglia function, suggesting that stimulation was sufficiently restricted to MSNs of either pathway.

Author Manuscript Author Manuscript Author Manuscript Author Manuscript

Furthermore, they confirm that the whole-brain networks recruited by light delivery and ultimately visualized with ofMRI are of behavioral significance.

Direct and indirect pathway stimulations evoke distinct brain-wide responses

To investigate how selective drive of the direct or indirect pathways differentially affect the basal ganglia-thalamocortical loop, we next coupled optogenetic D1- or D2-MSN stimulation to whole-brain fMRI readouts. Experiments were performed under very light anesthesia (0.4–0.7% isoflurane) to minimize suppression of neuronal activity. To facilitate imaging under these conditions and reduce motion artifacts, mice were gradually introduced to the fMRI-related environment, including noise and body restriction, over the course of 14 days. Following this habituation process, stable fMRI images could be acquired. For each scan, a 20 s pulse train of 20 Hz stimulation was delivered to the dorsomedial striatum every minute for six minutes. Significantly modulated voxels were identified as those whose time series were synchronized to consecutive periods of light delivery using standard Fourier domain techniques. There was typically more than a 5 dB difference in magnitude between the fundamental frequency of each region's time series and its higher harmonics, suggesting that this approach yielded few false negatives (Figure S1). Visualization of modulated, or "active", voxels revealed that both D1- and D2-MSN stimulation resulted in widespread modulation of brain activity (Figure 1D,H). Furthermore, the phase of evoked responses dramatically differed across stimulation groups and brain regions, indicating significant heterogeneity of the time series' temporal dynamics.

To quantify the extent of brain-wide activation patterns, we segmented the brain into 30 anatomically defined regions (Figure 2), giving a total of 60 regions of interest (ROIs) across both hemispheres. We next calculated the percentage of each ROI that exhibited significantly modulated fMRI time series (Figure 3). Regions with significant activation included not only those within the basal ganglia-thalamocortical loop, but also those within the limbic system and midbrain. Cortical activation was especially widespread, covering all segmented regions from frontal cortex (most anterior) to visual and parahippocampal cortex (most posterior). Contralateral activation was also common.

To explore the effect of stimulation on the basal ganglia-thalamocortical loop, we next examined fMRI time series of the various basal ganglia nuclei, thalamus, and motor cortex. Within the anterior caudate putamen, where stimulation was delivered, the BOLD signal was positive during stimulation of either population (Figure 4). At all other regions of the ipsilateral basal ganglia-thalamocortical loop – including GPe, STN, GPi, SN, thalamus, and motor cortex – the evoked response in a given region exhibited qualitatively different temporal profiles between D1- and D2-MSN stimulation (Figure 4). In general, positive responses were evoked during D1-MSN stimulation, while negative responses were evoked during D2-MSN stimulation. To quantify these differences in temporal patterns, we compared the average phase of active voxels within each ROI. This value represents the temporal shift of the sinusoid that best fits the modeled data in the least-squares sense (Figure 5A). The average phase of modulated voxels at the anterior caudate putamen was not significantly different between D1- and D2-MSN stimulations (Figure 5B,C; $p > 0.05$, circular Watson-Williams test). In contrast, the evoked responses in GPe, GPi, STN, SN,

Author Manuscript Author Manuscript Author Manuscript Author Manuscript

thalamus, and motor cortex were all significantly different (Figure 5B,C; $p < 0.001$, circular Watson-Williams test). To determine if the difference observed in motor cortex was generalizable across cortical activations, we also computed phases in the eleven other segmented ROIs of cortex. These too were significantly different between D1- and D2-MSN stimulations (Figure 5B,C), pointing to the widespread divergent influence of direct and indirect pathways. Time series for each cortical region ipsilateral to stimulation are shown in Figure S2. Importantly, similar differences in temporal dynamics were also observed in the contralateral hemisphere (Figuress S3 and S4).

To further characterize the evoked responses, we next calculated the integral of each ROI's time series (ΣBOLD). With the exception of the anterior caudate putamen, all ipsilateral ROIs exhibited a positive mean ΣBOLD value during D1-MSN stimulation and a negative mean ΣBOLD value during D2-MSN stimulation (Figure 5D). This difference was significant across most tested ROIs, including the basal ganglia's output nuclei GPi and SN, thalamus, and 10 of 12 segmented cortical regions ($p < 0.05$; two-tailed t-test). ΣBOLD was also generally positive during D1-MSN stimulation and negative during D2-MSN stimulation in the contralateral hemisphere (Figure S3D). This difference was significant across all contralateral regions of the basal ganglia (with the exception of the putamen) and 7 of 12 cortical regions ($p < 0.05$; two-tailed t-test).

Neuronal underpinnings of opposing fMRI responses

Given the diversity of BOLD responses evoked by D1- and D2-MSN stimulations, we next sought to verify whether the BOLD responses reflected underlying neuronal activity. Specifically, we sought to confirm that the opposing influences of the direct and indirect pathways measured on the macroscopic scale with ofMRI were also present at the level of single-unit activity. Thus, we performed extracellular recordings in striatum and thalamus (Figure 6A,E), where the differences between D1- and D2-MSN stimulation-evoked responses were least and most significant, respectively (Figure 5C), and where the sign of ΣBOLD was the same and opposite between the two stimulation groups, respectively (Figure 5D). Although the striatal BOLD response evoked by D2-MSN stimulation was larger in magnitude than the response evoked by D1-MSN stimulation, both time series exhibited clear and consistent increases upon 20 Hz light delivery (Figure 6B). Peri-event histograms from two representative neurons show that the increase in BOLD evoked by stimulation of either pathway was associated with increases in firing rate over repeated trials (Figure 6C). Indeed, virtually all recorded units exhibited significant increases in firing rate (Figure 6D; $p < 0.05$ for $n = 144/144$ units over 6 animals and 122/123 units over 5 animals for D1- and D2-MSN stimulation, respectively; one-tailed paired t-tests).

Unlike the BOLD signals observed at the site of stimulation in striatum, the fMRI BOLD signals in thalamus exhibited opposite responses during D1- and D2-MSN stimulation. Specifically, the evoked time series exhibited robust and reliable increases and decreases upon D1- and D2-MSN stimulation, respectively (Figure 6F). Electrophysiology recordings in thalamus were targeted to the ventrolateral nucleus, due to its established role in motor control (Figure 6E). Peri-event time histograms from two representative neurons show that these changes were associated with corresponding changes in neuronal activity that could be

Author Manuscript Author Manuscript Author Manuscript Author Manuscript

consistently driven over many repeated trials (Figure 6G). Indeed, across all recorded neurons in the thalamus, 94% of single-units exhibited an increase in firing rate during D1-MSN stimulation, while only 1% of units exhibited a decrease in firing rate (Figure 6H; $p < 0.05$ for $n = 107$ and 1 out of 114 units, respectively, over 8 animals; one-tailed paired t-tests). The remaining 5% (6/114 units) exhibited no significant change between the pre-stimulation and stimulation periods. During D2-MSN stimulation, only 1% of recorded units exhibited an increase in firing rate ($p < 0.05$ for $n = 1/70$ units over 5 animals; one-tailed paired t-tests). In agreement with the fMRI BOLD signal, however, 79% of cells exhibited a decrease in firing rate during D2-MSN stimulation (Figure 6H; $p < 0.05$ for $n = 55/70$ units over 5 animals; one-tailed paired t-tests). The remaining 20% (14/70 units) exhibited no significant change between the pre-stimulation and stimulation periods. Thus, the widespread opposing influences of direct and indirect pathways on thalamic activity measured with ofMRI were also present at a neuronal level.

Finally, we sought to verify the relationship between BOLD and neuronal activity in the STN and GPi – two regions where the evoked fMRI response was at odds with the classical feedforward model of direct and indirect pathways. The STN exhibited a positive signal during D1-MSN stimulation despite its presumed lack of involvement in the direct pathway, and a negative signal during D2-MSN stimulation, despite the increase in firing that is expected from its GPe-mediated disinhibition (Figure 7B). Similarly, the GPi exhibited positive and negative signals during D1- and D2-MSN stimulation, despite its expected decrease and increase in GABAergic output, respectively (Figure 7F). Therefore, to investigate whether these fMRI signals reflected underlying neuronal activity, we performed i*n vivo* extracellular recordings at each region during optical stimulation of striatal D1- and D2-MSNs (Figure 7A,E).

In agreement with the observed BOLD responses, the majority of modulated cells recorded in STN exhibited an increase in firing rate during D1-MSN stimulation and a decrease in firing rate during D2-MSN stimulation. 37% of units were excited by D1-MSN stimulation, with the remaining 63% exhibiting no significant change (Figure 7D; $n = 52$ units, 2 animals; one-sided t-test). Conversely, during D2-MSN stimulation, 76% of units were inhibited, 7% was excited, and 17% exhibited no change (Figure 7D; $n = 46$ units, 2 animals; one-sided t-test). These changes could be consistently driven over many repeated trials (Figure 7C). Importantly, the polarity of changes in neuronal activity also matched the polarity of BOLD modulations within the GPi. During D1-MSN stimulation, 34% of GPi units exhibited an increase in firing rate, with the remaining 66% exhibiting no significant change (Figure 7H; $n = 59$ units, 3 animals; one-sided t-test). During D2-MSN stimulation, 100% of recorded units exhibited a decrease in firing rate (Figure 7H; $n = 40$ units, 2 animals). Again, these changes were consistent over many repeated trials, using the same 20 s on – 40 s off paradigm employed during ofMRI studies (Figure 7G).

Discussion

In this study, we applied the optogenetic fMRI toolbox to investigate the effect of direct and indirect pathway stimulation on brain-wide circuit dynamics. The classical feedforward model of basal ganglia circuit function predicts that direct pathway (D1-MSN) activation

Author Manuscript Author Manuscript Author Manuscript Author Manuscript

results in disinhibition of the thalamus and subsequent activation of the thalamocortical loop (Albin et al., 1989). On the other hand, indirect pathway (D2-MSN) activation is predicted to increase the basal ganglia's inhibitory control over thalamus and therefore decrease activity of thalamus and cortex. Consistent with this view, we found that direct pathway activation led to positive fMRI responses in thalamus and motor cortex, while activation of the indirect pathway led to negative fMRI responses in these two regions. The fMRI responses to D1- and D2-MSN stimulation also exhibited opposite polarity in the basal ganglia's output nuclei (GPi and SN), STN, and various other regions of cortex (Figure 5D). Importantly, the opposing influence of direct and indirect pathways observed with fMRI in thalamus, GPi, and STN were associated with corresponding changes in neuronal activity. Our findings therefore support the proposed roles of the direct and indirect pathways in driving opposite brain-wide activity.

Although the classical feedforward basal ganglia model puts forth opposing roles for the direct and indirect pathways, recent studies have challenged this basic assumption (Calabresi et al., 2014; Cui et al., 2013). For example, one study identified a mixed population of excited and inhibited neurons in SNr during optogenetic stimulation of either D1- or D2-MSNs (Freeze et al., 2013). Given the projection from SNr to thalamus, it remained uncertain what the response of downstream thalamocortical regions would be. Our study confirms that the thalamus and cortex exhibit not only opposite responses, but responses that are in agreement with action initiation and suppression during direct and indirect pathway activation, respectively. These findings provide mechanistic insight for and support previous reports that bilateral stimulation of the direct pathway increases ambulation in mice, while bilateral stimulation of the indirect pathway reduces ambulation and increases freezing (Freeze et al., 2013; Kravitz et al., 2010). They also support the recent finding that D1-MSN, but not D2-MSN, stimulation acts as a "go" signal for goal-directed sensorimotor transformation (Sippy et al., 2015).

Interestingly, the sign of the fMRI BOLD response within the basal ganglia itself did not strictly follow the changes in neuronal activity predicted from the classical feedforward connections of direct or indirect pathways (Albin et al., 1989). In particular, the GPi and STN exhibited positive BOLD signals during direct pathway stimulation and negative BOLD signals during indirect pathway stimulation. These differences, which were found to reflect underlying neuronal activity (Figure 7), suggest that the circuit dynamics within basal ganglia during sustained (20 s) stimulation may be principally driven by feedback and non-canonical pathways. For example, the hyperdirect pathway, which includes glutamatergic projections from motor-related areas of cortex to STN (Monakow et al., 1978; Nambu et al., 2002), may explain the changes in STN during D1- and D2-MSN stimulation. According to this model, the positive STN response during direct pathway stimulation results from an increase in excitatory input from cortex, while the negative response during indirect pathway stimulation results from a decrease in excitatory input from cortex. If the hyperdirect pathway is indeed responsible for driving subthalamic activity, it then follows that the GPi, which receives strong excitatory input from STN, would also exhibit positive and negative responses during D1- and D2-MSN stimulation. The presence of inhibitory interneurons with local synapses and projection neurons with lateral connections throughout the basal ganglia nuclei – including striatum, GPe, STN, and SNr (Oorschot, 2010) – offers another

Author Manuscript Author Manuscript Author Manuscript Author Manuscript

potential explanation for why the observed responses in STN and GPi diverge from the classical model's theoretical predictions. For example, after finding that D1- and D2-MSN stimulations excite and inhibit a subset of SNr neurons, respectively, Freeze et al. (2013) hypothesized that these non-classical dynamics may result from the relief and activation of lateral inhibition formed by the local synapses of projection neurons.

Given the GPi's GABAergic control over thalamus, it may come as a surprise that both regions were excited and inhibited together during D1- and D2-MSN stimulation, respectively. According to the direct and indirect pathway model, the thalamus should respond in the opposite direction of the basal ganglia's output nuclei. One attractive explanation for this result is that thalamo-cortico-thalamic circuits help sustain the predicted responses in thalamus and cortex at steady state, while feedback connections and local circuitry drive the basal ganglia. Indeed, evidence suggests that cortico-thalamic projections exhibit non-reciprocal connections with the basal ganglia relay nuclei in thalamus (McFarland and Haber, 2002), providing an anatomical substrate for the widespread recruitment of thalamus and cortex we observed.

Importantly, these proposed mechanisms are still compatible with the engagement of pathways that have a functional influence in opposition to what was observed with fMRI. For example, GABAergic input from striatum will still inhibit the GPi during D1-MSN stimulation. However, our results suggest that this may not be the dominant pathway in driving GPi activity at steady state. Indeed, the complexity of excitatory and non-excitatory connections within the basal ganglia-thalamocortical circuit makes the outcome of sustained D1- or D2-MSN stimulation on each region's activity difficult to predict. We show that ofMRI is a powerful tool to measure these unpredictable responses and identify the relative influence of different pathways within the whole-brain circuit during a local, cell type-specific perturbation.

The use of electrophysiology recordings alone to measure the activity of a single region presents a limited perspective on D1- or D2-MSN stimulation's effect on network-level brain circuits. Exploiting fMRI's large field-of-view in these experiments allowed us to simultaneously visualize the whole-brain influence of direct or indirect pathway stimulation. This is particularly important given the basal ganglia's widespread influence on the cerebral cortex. In non-human primates, for example, closed-loop circuits between the basal ganglia and motor cortex, prefrontal cortex, and cingulate/orbitofrontal cortex are involved in skeletomotor, cognitive, and limbic functions, respectively (Alexander et al., 1990; Alexander et al., 1986). These pathways are generally thought to be topographically segregated within the striatum, although exact boundaries are a subject of debate (Voorn et al., 2004). In general, however, the dorsal striatum is typically associated with sensorimotor function, while the ventral striatum is associated with processing limbic information. It is perhaps surprising then that spatially restricted stimulation of either D1- or D2-MSNs in the dorsomedial striatum evoked widespread fMRI activations throughout cortex and thalamus (Figure 1D,H and Figure 3). This massive scale of activation suggests that basal ganglia output within the beta frequency band does not necessarily propagate through the thalamocortical loop via functionally distinct circuits. It has been suggested that communication between these circuits is supported by non-reciprocal corticothalamic

Author Manuscript Author Manuscript Author Manuscript Author Manuscript

connections and laminar-specific thalamocortical projections (McFarland and Haber, 2002). These projections may thus serve as the anatomical substrate underlying the propagation of stimulus-driven activity throughout the brain during D1- and D2-MSN stimulations. It is also important to note that beta oscillations are known to regulate long-range cortico-cortical synchronizations (Schnitzler and Gross, 2005). Stimulation at 20 Hz may therefore cause widespread cortical synchronization and lead to fMRI modulations in diverse regions of cortex.

Beyond the basal ganglia-thalamocortical circuit, the results of our experiment provide important insight into the cellular origins of the BOLD signal. While significant progress has been made on understanding neurovascular coupling and the relationship between BOLD signals and neuronal activity (Bandettini, 2014; Bandettini et al., 1992; Huettel et al., 2004; Huttunen et al., 2008; Kilner et al., 2005; Logothetis, 2008; Wang et al., 2012), it remains unknown how different cell populations contribute to this effect. Early optogenetic fMRI studies helped address this issue, showing that selectively driving excitatory neurons in cortex, hippocampus, and thalamus evoke local positive BOLD signals (Desai et al., 2011; Duffy et al., 2015; Kahn et al., 2013; Lee et al., 2010; Liu et al., 2015; Weitz et al., 2015). However, fMRI signals arising from predominately non-excitatory regions like the striatum remain difficult to interpret. For example, it has been shown that inhibitory neuron activity is accompanied by changes in blood flow and glucose metabolism (Buzsaki et al., 2007; Lauritzen and Gold, 2003), while another study concluded that the net activity of inhibitory Purkinje cells in cerebellum is unimportant for the vascular response (Mathiesen et al., 1998). Most recently, it was shown that targeted excitation of parvalbumin-expressing interneurons locally evokes positive BOLD signals with neighboring negative BOLD signals (Lee et al., 2010). Yet because these interneurons were interspersed within the predominately excitatory network of cortex, their specific contribution could not be easily determined. Here, we demonstrate that targeted activations of inhibitory D1- and D2-MSNs in striatum separately evoke local positive BOLD responses (Figure 6B). Given that 90–95% of cells in striatum are inhibitory MSNs (Gerfen, 2004; Kemp and Powell, 1971), the increase in striatal BOLD signal likely reflects the spiking activity of these GABAergic neurons. An alternative explanation might be that the observed increase in signal is due to synaptic input from cortex (Logothetis, 2003; Logothetis et al., 2001). However, the expected reduction in glutamatergic input from thalamus and cortex to striatum during D2-MSN stimulation renders the first explanation more likely. The increase in BOLD might also reflect changes in the input of striatal interneurons, but these constitute only a fraction of the local population (<10%). These data therefore strongly suggest that spiking of GABAergic neurons causes a local positive BOLD response. This interpretation can be easily extended to the many human fMRI studies that observed increases in the striatal BOLD signal during reward-related stimuli (Breiter et al., 1997; Carlson et al., 2011; Risinger et al., 2005), learning (Rauch et al., 1997), and memory cues (Lewis et al., 2004). Specifically, our findings suggest it is possible that these increases reflect activation of striatal neurons, and not simply an increase in synaptic input or local processing.

The combination of fMRI with brain stimulation – both optogenetic and electrical – offers a powerful tool for visualizing the dynamic nature of brain circuits (Abe et al., 2012; Canals et al., 2008; Desai et al., 2011; Duffy et al., 2015; Ferenczi et al., 2016; Field et al., 2008; Lee

Author Manuscript Author Manuscript Author Manuscript Author Manuscript

et al., 2010; Liu et al., 2015; Paek et al., 2015; Tolias et al., 2005; Weitz et al., 2015). Interpretation of evoked signals, however, often relies on an understanding of underlying circuitry. Determining to what extent stimulation-evoked BOLD responses can reflect polysynaptic propagation has therefore been a central question within the field of fMRI. While the majority of combined fMRI-stimulation studies report BOLD activation in monosynaptically connected regions (Ekstrom et al., 2008; Gerits et al., 2012; Matsui et al., 2011; Ohayon et al., 2013), several studies employing electrical microstimulation in thalamus and cortex have demonstrated that stimulation effects can also spread to generate remote BOLD signals across multiple synapses (Matsui et al., 2012; Murayama et al., 2011). We add to this body of literature, showing that targeted stimulations of striatum generate BOLD signals not only in the monosynaptically connected nuclei of basal ganglia, but also in regions two or three synapses away, such as thalamus and cortex. Remarkably, these signals exhibited polarities in agreement with the increases and decreases in neuronal activity predicted from stimulation of D1- or D2-MSNs after tracing their inhibitory projections through the basal ganglia's inhibitory output. These data illustrate the power of the fMRI BOLD signal in accurately capturing whole-brain dynamics through complex circuits that include excitatory and inhibitory connections alike.

Experimental Procedures

Subjects

Two bacterial artificial chromosome (BAC)-mediated transgenic mouse lines from GENSAT (Gong et al., 2003) were used in this study: BAC-Cre Drd1a-262 and BAC-Cre Drd2-44. Mice expressed Cre-recombinase under control of either the D1 dopamine receptor (n = 32 total) or D2 dopamine receptor (n = 27 total) regulatory elements. Male mice weighing 15–20 g (~4 weeks old) were used as subjects. Animals were housed individually following cannula implantation (see below) and provided with food and water *ad libitum*. All experimental procedures and animal husbandry were performed in strict accordance with the National Institutes of Health, UCLA Institutional Animal Care and Use Committee (IACUC), and Stanford University IACUC guidelines. Of the 32 D1-Cre mice injected in this study, 13 were used for imaging, 2 for immunohistochemistry, 6 for striatal recordings, 8 for thalamus recordings, and 3 for STN/GPi recordings. Of the 27 D2-Cre mice injected in this study, 11 were used for imaging, 4 for immunohistochemistry, 5 for striatal recordings, 5 for thalamus recordings, and 2 for STN/GPi recordings. Note that one of the original D1-Cre mice used for imaging exhibited negligible fMRI activity and no behavioral response to stimulation (measured in rotations per minute, see below). It was therefore eliminated from the study, leaving n = 12 D1-Cre mice for further fMRI analysis. Functional opsin expression was confirmed in all mice used for electrophysiology via a behavioral response to stimulation.

Viral Expression and Stereotaxic Surgery

A double-floxed inverted (DIO) recombinant AAV1 virus was used to express ChR2-EYFP in Cre-expressing neurons. The double-floxed reverse ChR2-EYFP cassette was cloned into a modified version of the pAAV2-MCS vector (Stratagene, La Jolla, CA) carrying the EF-1α promoter and WPRE to enhance expression. The recombinant AAV vector was serotyped

Author Manuscript Author Manuscript Author Manuscript Author Manuscript

with AAV1 coat proteins and packaged by the University of North Carolina viral vector core (titer of 4×10^{12} particles/ml). During surgery, animals were anesthetized with isoflurane (induction 5%, maintenance 1.5–2%; Sigma-Aldrich, St. Louis, Missouri, USA) and secured in a stereotactic frame (Kopf Instruments). A heating pad was used to maintain body temperature, and artificial tears were applied to the eyes to prevent desiccation during surgery. Buprenorphine (0.05 mg/kg) was injected subcutaneously for analgesia. After a midline incision along the scalp, a small craniotomy and viral injection/cannula implantation were performed at the dorsomedial striatum (+0.48 mm AP, −1.5 mm ML, injection at +3.0 mm DV). 1 μl of the AAV1/DIO-ChR2-EYFP virus was delivered using a 10 μl syringe and 34 gauge metal needle (World Precision Instruments Inc., Sarasota, FL) at a 100 nl/min flow rate driven by a micro-syringe pump controller. The syringe needle was left in place for 5–10 minutes and then slowly withdrawn. A custom-designed fiber-optic cannula was next mounted and secured on the skull using metabond (Parkell Inc.), with the optical fiber extending from the cannula's base to the desired depth (~0.2 mm above the injection site). Following surgery, mice were given buprenorphine (0.05 mg/kg, s.c.) twice daily for 2 days to minimize post-operative discomfort. All experiments were conducted at least 3 weeks following virus injection to ensure optimal ChR2 expression. Probe locations were validated in all animals used for ofMRI experiments with T2-weighed structural MRI images.

Behavioral Analysis in Awake Mice

To validate functional ChR2 expression and successful control of the direct or indirect pathway, the rotational behavior of freely moving animals was quantified during stimulation of D1- or D2-MSNs. Animals were placed in a round arena (18.5 cm diameter), monitored with an overhead video camera, and left to acclimate for 15 min before recording. A series of 3–6 trials were performed with 20 s of photostimulation (20 Hz with a 30% duty cycle) followed by 40 s without stimulation. Light was delivered via a 105 μm diameter optical fiber connected to a 473 nm laser source (Laserglow Technologies, Toronto, Canada). Video recording started 40 s prior to the first stimulation. For each trial, the number and direction of rotations – defined by a full 360° turn in one direction without more than a 90° turn in the opposite direction – were quantified for the periods with and without stimulation, and the number of rotations per minute was calculated. All video recordings were scored blindly.

ofMRI Experiments and fMRI Data Analysis

fMRI scanning was performed using a 7 Tesla Bruker Biospec small animal MRI system. To facilitate fMRI scanning under very light anesthesia (0.4–0.7% isoflurane mixed with O2 and N2O), mice were gradually introduced to fMRI-related phenomena and rewarded with peanut butter over the course of 14 days. A single ofMRI scan consisted of six 20 s pulse trains of optical stimulation delivered once per minute over 6 min. Stimulation parameters were the same as those used for behavior (20 Hz, 30% duty cycle, 2.5 mW via a 105 μm diameter optical fiber). Voxels whose time series were significantly modulated by optogenetic stimulation were identified using Fourier domain techniques (Bandettini et al., 1993). Regions of interest were based on a published MRI mouse atlas (http://www.bioeng.nus.edu.sg/cfa/mouse_atlas.html) (Bai et al., 2012) that was corrected to include all regions of the basal ganglia and cortex by aligning the anatomical template to a

Author Manuscript Author Manuscript Author Manuscript Author Manuscript

digital mouse atlas (Paxinos and Franklin, 2001). Further details on acclimation, the fMRI experiment, and data analysis are provided in the Supplemental Experimental Procedures.

In Vivo Extracellular Electrophysiology

Single unit recordings were conducted at select sites modulated by light stimulation during ofMRI to assess the underlying neural activity. After exposing and cleaning the skull, an additional craniotomy was made above the desired recording site. An acute 16-channel microelectrode array (NeuroNexus Technologies, model A1×16–5mm-25–177-A16) was targeted to the recording site using stereotaxic instruments. As with behavior and ofMRI experiments, the implanted fiber-optic cannula in striatum was connected to a 473 nm laser source with an output power level of 2.5 mW via a 105 μm diameter optical fiber. Animals were anesthetized with 0.6–0.8% isoflurane through a nose cone during recordings. Plexon's omniplex system and plexcontrol software were used to capture and sort the spike waveform data in real-time. Recordings were collected for 20 s without stimulation, followed by repeated stimulation cycles (20 s on, 40 s off). Threshold search and principal component analysis in Plexon's Offline Sorter application were used for automated detection of single-unit spikes within multi-unit recordings. Thresholds were validated by visual inspection and modified if necessary. For traces with multiple spike populations, thresholds were set to capture all the spikes. The following coordinates represent the average recording location across animals, when exact coordinates were available: +0.52 mm AP, −1.64 mm ML, +3.33 mm DV (striatum, n = 10 of 11 animals), −1.32 mm AP, −1.08 mm ML, +3.58 mm DV (thalamus, n = 9 of 13 animals), −2.06 mm AP, −1.39 mm ML, +4.54 mm DV (STN, n = 4 of 4 animals), −1.34 mm AP, −1.73 mm ML, +4.37 mm DV (GPi, n = 5 of 5 animals). Thalamic recordings were targeted to the ventrolateral (VL) motor nucleus.

Opsin Expression Validation

Immunohistochemistry was performed to assess the specificity of ChR2-EYFP expression to dopaminergic D1- and D2-MSNs. Full details are provided in the Supplemental Experimental Procedures.

General Statistics

All statistical comparisons were performed in the Matlab software environment (MathWorks, Inc., Natick, MA). Circular statistics were performed using the CircStat toolbox (Berens, 2009). Statistical significance for all tests was determined using a threshold of $\alpha = 0.05$.

Supplementary Material

Refer to Web version on PubMed Central for supplementary material.

Acknowledgments

This work was supported by the NIH/NIBIB R00 Award (R00EB008738), Okawa Foundation Research Grant Award, NIH Director's New Innovator Award (DP2OD007265), the NSF CAREER Award (1056008), the Alfred P. Sloan Research Fellowship, and the NIH/NINDS R01 (R01NS091461).

Author Manuscript Author Manuscript Author Manuscript Author Manuscript

References

Abe Y, Sekino M, Terazono Y, Ohsaki H, Fukazawa Y, Sakai S, Yawo H, Hisatsune T. Opto-fMRI analysis for exploring the neuronal connectivity of the hippocampal formation in rats. Neuroscience research. 2012; 74:248–255. [PubMed: 22982343]

Albin RL, Young AB, Penney JB. The functional anatomy of basal ganglia disorders. Trends in neurosciences. 1989; 12:366–375. [PubMed: 2479133]

Alexander GE, Crutcher MD, DeLong MR. Basal ganglia-thalamocortical circuits: parallel substrates for motor, oculomotor, “prefrontal” and “limbic” functions. Progress in brain research. 1990; 85:119–146. [PubMed: 2094891]

Alexander GE, DeLong MR, Strick PL. Parallel organization of functionally segregated circuits linking basal ganglia and cortex. Annual review of neuroscience. 1986; 9:357–381.

Bai J, Trinh TL, Chuang KH, Qiu A. Atlas-based automatic mouse brain image segmentation revisited: model complexity vs. image registration. Magnetic resonance imaging. 2012; 30:789–798. [PubMed: 22464452]

Bandettini PA. Neuronal or hemodynamic? Grappling with the functional MRI signal. Brain connectivity. 2014; 4:487–498. [PubMed: 25093397]

Bandettini PA, Jesmanowicz A, Wong EC, Hyde JS. Processing strategies for time-course data sets in functional MRI of the human brain. Magn Reson Med. 1993; 30:161–173. [PubMed: 8366797]

Bandettini PA, Wong EC, Hinks RS, Tikofsky RS, Hyde JS. Time course EPI of human brain function during task activation. Magn Reson Med. 1992; 25:390–397. [PubMed: 1614324]

Berens P. CircStat: A MATLAB Toolbox for Circular Statistics. J Stat Softw. 2009; 31:1–21.

Breiter HC, Gollub RL, Weisskoff RM, Kennedy DN, Makris N, Berke JD, Goodman JM, Kantor HL, Gastfriend DR, Riorden JP, et al. Acute effects of cocaine on human brain activity and emotion. Neuron. 1997; 19:591–611. [PubMed: 9331351]

Buzsaki G, Kaila K, Raichle M. Inhibition and brain work. Neuron. 2007; 56:771–783. [PubMed: 18054855]

Calabresi P, Picconi B, Tozzi A, Ghiglieri V, Di Filippo M. Direct and indirect pathways of basal ganglia: a critical reappraisal. Nat Neurosci. 2014; 17:1022–1030. [PubMed: 25065439]

Canals S, Beyerlein M, Murayama Y, Logothetis NK. Electric stimulation fMRI of the perforant pathway to the rat hippocampus. Magnetic resonance imaging. 2008; 26:978–986. [PubMed: 18479870]

Carlson JM, Foti D, Mujica-Parodi LR, Harmon-Jones E, Hajcak G. Ventral striatal and medial prefrontal BOLD activation is correlated with reward-related electrocortical activity: a combined ERP and fMRI study. Neuroimage. 2011; 57:1608–1616. [PubMed: 21624476]

Cazorla M, de Carvalho FD, Chohan MO, Shegda M, Chuhma N, Rayport S, Ahmari SE, Moore H, Kellendonk C. Dopamine D2 receptors regulate the anatomical and functional balance of basal ganglia circuitry. Neuron. 2014; 81:153–164. [PubMed: 24411738]

Cui G, Jun SB, Jin X, Pham MD, Vogel SS, Lovinger DM, Costa RM. Concurrent activation of striatal direct and indirect pathways during action initiation. Nature. 2013; 494:238–242. [PubMed: 23354054]

DeLong MR. Primate models of movement disorders of basal ganglia origin. Trends in neurosciences. 1990; 13:281–285. [PubMed: 1695404]

Deng YP, Lei WL, Reiner A. Differential perikaryal localization in rats of D1 and D2 dopamine receptors on striatal projection neuron types identified by retrograde labeling. J Chem Neuroanat. 2006; 32:101–116. [PubMed: 16914290]

Desai M, Kahn I, Knoblich U, Bernstein J, Atallah H, Yang A, Kopell N, Buckner RL, Graybiel AM, Moore CI, et al. Mapping brain networks in awake mice using combined optical neural control and fMRI. J Neurophysiol. 2011; 105:1393–1405. [PubMed: 21160013]

Duffy BA, Choy M, Chuapoco MR, Madsen M, Lee JH. MRI compatible optrodes for simultaneous LFP and optogenetic fMRI investigation of seizure-like afterdischarges. Neuroimage. 2015; 123:173–184. [PubMed: 26208873]

Author Manuscript Author Manuscript Author Manuscript Author Manuscript

Ekstrom LB, Roelfsema PR, Arsenault JT, Bonmassar G, Vanduffel W. Bottom-up dependent gating of frontal signals in early visual cortex. Science. 2008; 321:414–417. [PubMed: 18635806]

Ferenczi EA, Zalocusky KA, Liston C, Grosenick L, Warden MR, Amatya D, Katovich K, Mehta H, Patenaude B, Ramakrishnan C, et al. Prefrontal cortical regulation of brainwide circuit dynamics and reward-related behavior. Science. 2016; 351:aac9698. [PubMed: 26722001]

Field CB, Johnston K, Gati JS, Menon RS, Everling S. Connectivity of the primate superior colliculus mapped by concurrent microstimulation and event-related FMRI. PloS one. 2008; 3:e3928. [PubMed: 19079541]

Freeze BS, Kravitz AV, Hammack N, Berke JD, Kreitzer AC. Control of basal ganglia output by direct and indirect pathway projection neurons. J Neurosci. 2013; 33:18531–18539. [PubMed: 24259575]

Gerfen, CR. Basal Ganglia. In: Paxinos, G., editor. The Rat Nervous System (Third Edition). Burlington: Academic Press; 2004. p. 455-508.

Gerfen CR, Engber TM, Mahan LC, Susel Z, Chase TN, Monsma FJ Jr, Sibley DR. D1 and D2 dopamine receptor-regulated gene expression of striatonigral and striatopallidal neurons. Science. 1990; 250:1429–1432. [PubMed: 2147780]

Gerits A, Farivar R, Rosen BR, Wald LL, Boyden ES, Vanduffel W. Optogenetically induced behavioral and functional network changes in primates. Current biology : CB. 2012; 22:1722–1726. [PubMed: 22840516]

Gong S, Doughty M, Harbaugh CR, Cummins A, Hatten ME, Heintz N, Gerfen CR. Targeting Cre recombinase to specific neuron populations with bacterial artificial chromosome constructs. J Neurosci. 2007; 27:9817–9823. [PubMed: 17855595]

Gong S, Zheng C, Doughty ML, Losos K, Didkovsky N, Schambra UB, Nowak NJ, Joyner A, Leblanc G, Hatten ME, et al. A gene expression atlas of the central nervous system based on bacterial artificial chromosomes. Nature. 2003; 425:917–925. [PubMed: 14586460]

Huettel SA, McKeown MJ, Song AW, Hart S, Spencer DD, Allison T, McCarthy G. Linking hemodynamic and electrophysiological measures of brain activity: evidence from functional MRI and intracranial field potentials. Cerebral cortex. 2004; 14:165–173. [PubMed: 14704213]

Huttunen JK, Grohn O, Penttonen M. Coupling between simultaneously recorded BOLD response and neuronal activity in the rat somatosensory cortex. Neuroimage. 2008; 39:775–785. [PubMed: 17964186]

Kahn I, Knoblich U, Desai M, Bernstein J, Graybiel AM, Boyden ES, Buckner RL, Moore CI. Optogenetic drive of neocortical pyramidal neurons generates fMRI signals that are correlated with spiking activity. Brain Res. 2013; 1511:33–45. [PubMed: 23523914]

Kemp JM, Powell TP. The structure of the caudate nucleus of the cat: light and electron microscopy. Philos Trans R Soc Lond B Biol Sci. 1971; 262:383–401. [PubMed: 4107495]

Kilner JM, Mattout J, Henson R, Friston KJ. Hemodynamic correlates of EEG: a heuristic. Neuroimage. 2005; 28:280–286. [PubMed: 16023377]

Kravitz AV, Freeze BS, Parker PR, Kay K, Thwin MT, Deisseroth K, Kreitzer AC. Regulation of parkinsonian motor behaviours by optogenetic control of basal ganglia circuitry. Nature. 2010; 466:622–626. [PubMed: 20613723]

Kravitz AV, Tye LD, Kreitzer AC. Distinct roles for direct and indirect pathway striatal neurons in reinforcement. Nat Neurosci. 2012; 15:816–818. [PubMed: 22544310]

Lauritzen M, Gold L. Brain function and neurophysiological correlates of signals used in functional neuroimaging. J Neurosci. 2003; 23:3972–3980. [PubMed: 12764081]

Lee JH, Durand R, Gradinaru V, Zhang F, Goshen I, Kim DS, Fenno LE, Ramakrishnan C, Deisseroth K. Global and local fMRI signals driven by neurons defined optogenetically by type and wiring. Nature. 2010; 465:788–792. [PubMed: 20473285]

Lewis SJ, Dove A, Robbins TW, Barker RA, Owen AM. Striatal contributions to working memory: a functional magnetic resonance imaging study in humans. Eur J Neurosci. 2004; 19:755–760. [PubMed: 14984425]

Liu J, Lee HJ, Weitz AJ, Fang Z, Lin P, Choy M, Fisher R, Pinskiy V, Tolpygo A, Mitra P. Frequency-selective control of cortical and subcortical networks by central thalamus. eLife. 2015; 4:e09215. [PubMed: 26652162]

Author Manuscript Author Manuscript Author Manuscript Author Manuscript

Lobo MK, Covington HE 3rd, Chaudhury D, Friedman AK, Sun H, Damez-Werno D, Dietz DM, Zaman S, Koo JW, Kennedy PJ, et al. Cell type-specific loss of BDNF signaling mimics optogenetic control of cocaine reward. Science. 2010; 330:385–390. [PubMed: 20947769]

Logothetis NK. The underpinnings of the BOLD functional magnetic resonance imaging signal. J Neurosci. 2003; 23:3963–3971. [PubMed: 12764080]

Logothetis NK. What we can do and what we cannot do with fMRI. Nature. 2008; 453:869–878. [PubMed: 18548064]

Logothetis NK, Pauls J, Augath M, Trinath T, Oeltermann A. Neurophysiological investigation of the basis of the fMRI signal. Nature. 2001; 412:150–157. [PubMed: 11449264]

Mailly P, Charpier S, Menetrey A, Deniau JM. Three-dimensional organization of the recurrent axon collateral network of the substantia nigra pars reticulata neurons in the rat. J Neurosci. 2003; 23:5247–5257. [PubMed: 12832549]

Matamales M, Bertran-Gonzalez J, Salomon L, Degos B, Deniau JM, Valjent E, Herve D, Girault JA. Striatal medium-sized spiny neurons: identification by nuclear staining and study of neuronal subpopulations in BAC transgenic mice. PloS one. 2009; 4:e4770. [PubMed: 19274089]

Mathiesen C, Caesar K, Akgoren N, Lauritzen M. Modification of activity-dependent increases of cerebral blood flow by excitatory synaptic activity and spikes in rat cerebellar cortex. J Physiol. 1998; 512(Pt 2):555–566. [PubMed: 9763643]

Matsui T, Koyano KW, Tamura K, Osada T, Adachi Y, Miyamoto K, Chikazoe J, Kamigaki T, Miyashita Y. FMRI activity in the macaque cerebellum evoked by intracortical microstimulation of the primary somatosensory cortex: evidence for polysynaptic propagation. PloS one. 2012; 7:e47515. [PubMed: 23118875]

Matsui T, Tamura K, Koyano KW, Takeuchi D, Adachi Y, Osada T, Miyashita Y. Direct comparison of spontaneous functional connectivity and effective connectivity measured by intracortical microstimulation: an fMRI study in macaque monkeys. Cerebral cortex. 2011; 21:2348–2356. [PubMed: 21368090]

McFarland NR, Haber SN. Thalamic relay nuclei of the basal ganglia form both reciprocal and nonreciprocal cortical connections, linking multiple frontal cortical areas. J Neurosci. 2002; 22:8117–8132. [PubMed: 12223566]

Miwa H, Fuwa T, Nishi K, Kondo T. Subthalamo-pallido-striatal axis: a feedback system in the basal ganglia. Neuroreport. 2001; 12:3795–3798. [PubMed: 11726797]

Monakow KH, Akert K, Kunzle H. Projections of the precentral motor cortex and other cortical areas of the frontal lobe to the subthalamic nucleus in the monkey. Experimental brain research. 1978; 33:395–403. [PubMed: 83239]

Murayama Y, Augath M, Logothetis NK. Activation of SC during electrical stimulation of LGN: retinal antidromic stimulation or corticocollicular activation? Magnetic resonance imaging. 2011; 29:1351–1357. [PubMed: 21920684]

Nambu A, Tokuno H, Takada M. Functional significance of the cortico-subthalamo-pallidal 'hyperdirect' pathway. Neuroscience research. 2002; 43:111–117. [PubMed: 12067746]

Ohayon S, Grimaldi P, Schweers N, Tsao DY. Saccade modulation by optical and electrical stimulation in the macaque frontal eye field. J Neurosci. 2013; 33:16684–16697. [PubMed: 24133271]

Oldenburg IA, Sabatini BL. Antagonistic but Not Symmetric Regulation of Primary Motor Cortex by Basal Ganglia Direct and Indirect Pathways. Neuron. 2015; 86:1174–1181. [PubMed: 26050037]

Oorschot DE. Cell types in the different nuclei of the basal ganglia. Handbook of basal ganglia structure and function. 2010; 20:63–74.

Paek SB, Min HK, Kim I, Knight EJ, Baek JJ, Bieber AJ, Lee KH, Chang SY. Frequency-dependent functional neuromodulatory effects on the motor network by ventral lateral thalamic deep brain stimulation in swine. Neuroimage. 2015; 105:181–188. [PubMed: 25451479]

Paxinos, G., Franklin, KB. The mouse brain in stereotaxic coordinates. 2. San Diego: Academic Press; 2001.

Rauch SL, Whalen PJ, Savage CR, Curran T, Kendrick A, Brown HD, Bush G, Breiter HC, Rosen BR. Striatal recruitment during an implicit sequence learning task as measured by functional magnetic resonance imaging. Hum Brain Mapp. 1997; 5:124–132. [PubMed: 10096417]

Author Manuscript Author Manuscript Author Manuscript Author Manuscript

Risinger RC, Salmeron BJ, Ross TJ, Amen SL, Sanfilipo M, Hoffmann RG, Bloom AS, Garavan H, Stein EA. Neural correlates of high and craving during cocaine self-administration using BOLD fMRI. Neuroimage. 2005; 26:1097–1108. [PubMed: 15886020]

Saunders A, Oldenburg IA, Berezovskii VK, Johnson CA, Kingery ND, Elliott HL, Xie T, Gerfen CR, Sabatini BL. A direct GABAergic output from the basal ganglia to frontal cortex. Nature. 2015; 521:85–89. [PubMed: 25739505]

Schnitzler A, Gross J. Normal and pathological oscillatory communication in the brain. Nat Rev Neurosci. 2005; 6:285–296. [PubMed: 15803160]

Sippy T, Lapray D, Crochet S, Petersen CC. Cell-Type-Specific Sensorimotor Processing in Striatal Projection Neurons during Goal-Directed Behavior. Neuron. 2015; 88:298–305. [PubMed: 26439527]

Smith Y, Raju DV, Pare JF, Sidibe M. The thalamostriatal system: a highly specific network of the basal ganglia circuitry. Trends in neurosciences. 2004; 27:520–527. [PubMed: 15331233]

Tolias AS, Sultan F, Augath M, Oeltermann A, Tehovnik EJ, Schiller PH, Logothetis NK. Mapping cortical activity elicited with electrical microstimulation using FMRI in the macaque. Neuron. 2005; 48:901–911. [PubMed: 16364895]

Voorn P, Vanderschuren LJ, Groenewegen HJ, Robbins TW, Pennartz CM. Putting a spin on the dorsal-ventral divide of the striatum. Trends in neurosciences. 2004; 27:468–474. [PubMed: 15271494]

Wang L, Saalmann YB, Pinsk MA, Arcaro MJ, Kastner S. Electrophysiological low-frequency coherence and cross-frequency coupling contribute to BOLD connectivity. Neuron. 2012; 76:1010–1020. [PubMed: 23217748]

Weitz AJ, Fang Z, Lee HJ, Fisher RS, Smith WC, Choy M, Liu J, Lin P, Rosenberg M, Lee JH. Optogenetic fMRI reveals distinct, frequency-dependent networks recruited by dorsal and intermediate hippocampus stimulations. Neuroimage. 2015; 107:229–241. [PubMed: 25462689]

Weitz AJ, Lee JH. Progress with optogenetic functional MRI and its translational implications. Future Neurology. 2013; 8:691–700.

Author Manuscript Author Manuscript Author Manuscript Author Manuscript

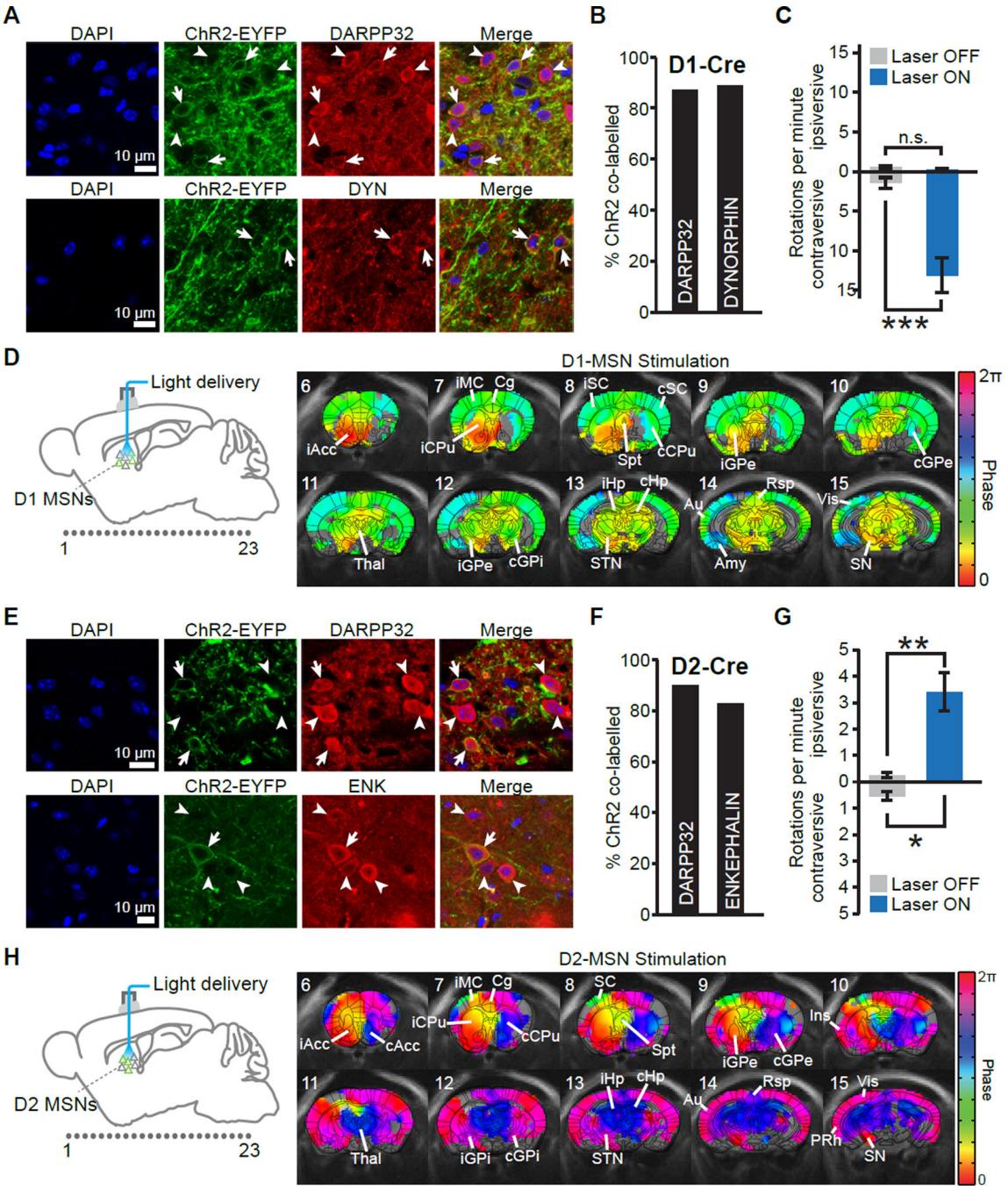

Figure 1. Combining optogenetic control of D1- and D2-MSNs with simultaneous fMRI readouts reveals robust distinct activity throughout the brain

A, Representative histology of ChR2-EYFP co-labelled with DARPP-32 (top) or dynorphin (bottom) in D1-Cre mice. Arrows indicate cells co-expressing ChR2-EYFP and the stained antibody. Arrowheads indicate ChR2-EYFP-negative cells expressing the stained antibody. **B**, Quantification of ChR2 and antibody co-localization in D1-Cre mice. 87% of ChR2-positive neurons were co-labelled with DARPP-32 (n = 2 mice, 150/172 cells), while 90% of ChR2-positive neurons co-localized with dynorphin (DYN; n = 2 mice, 135/150 cells). **C**, In

Author Manuscript Author Manuscript Author Manuscript Author Manuscript

behavioral tests with awake mice, the number of contraversive rotations per minute significantly increased during D1-MSN stimulation (n = 12 animals, *** $p < 0.001$ two-tailed paired t-test). **D**, Group-wise phase maps, masked to active voxels, of whole-brain fMRI responses evoked during D1-MSN stimulation (n = 12 animals). Dots numbered 1 through 23 on the left schematic indicate the location of coronal MRI slices. **E**, Representative histology of ChR2-EYFP co-labelled with DARPP-32 (top) or enkephalin (bottom) in D2-Cre mice. Arrows indicate cells co-expressing ChR2-EYFP and the stained antibody. Arrowheads indicate ChR2-EYFP-negative cells expressing the stained antibody. **F**, Quantification of ChR2 and antibody co-localization in D2-Cre mice. 89% of ChR2-positive neurons co-labelled with DARPP-32 (n = 2 mice, 119/133 cells), while 83% of ChR2-positive neurons were co-labelled with enkephalin (ENK; n = 4 mice, 190/228 cells). **G**, In behavioral tests with awake mice, the number of ipsiversive rotations per minute significantly increased during D2-MSN stimulation, while the number of contraversive rotations significantly decreased (n = 11 animals, * $p < 0.05$, ** $p < 0.005$; two-tailed paired t-test). **H**, Group-wise phase maps, masked to active voxels, of whole-brain fMRI responses evoked during D2-MSN stimulation (n = 11 animals). Dots numbered 1 through 23 on the left schematic indicate the location of coronal MRI slices. Abbreviations are as follows: Acc, accumbens; Amy, amygdala; Au, auditory cortex; CPu, caudate putamen; GPe, external globus pallidus; GPi, internal globus pallidus; Hp, hippocampus; MC, motor cortex; SC, sensory cortex; SN substantia nigra; Spt, septal nuclei; STN, subthalamic nucleus; Thal, thalamus; Vis, visual cortex. See also Figure S1.

Author Manuscript Author Manuscript Author Manuscript Author Manuscript

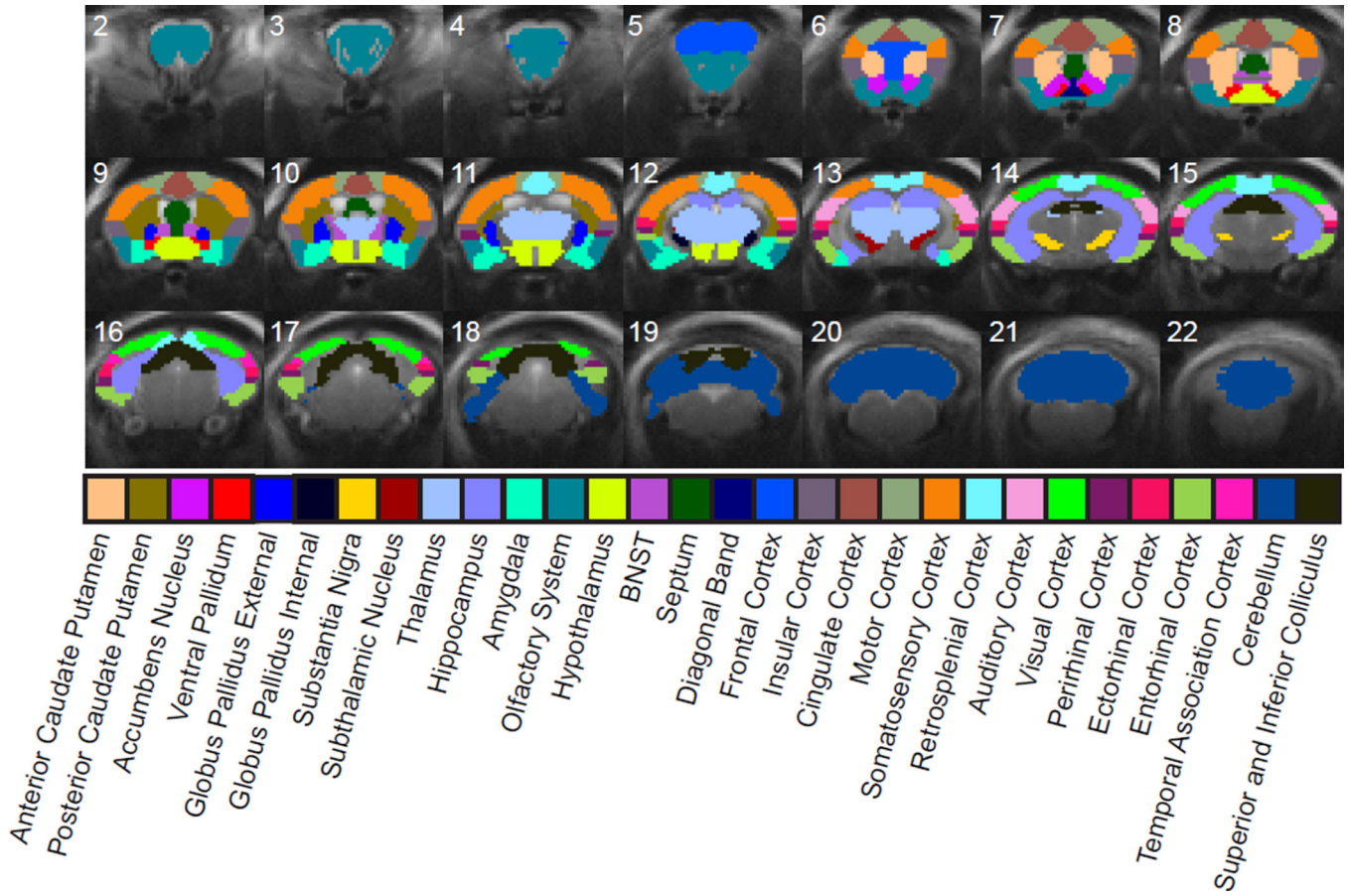

Figure 2. Brain-wide fMRI activations were segmented with anatomical regions of interest (ROIs) for quantitative analysis of spatiotemporal properties

Segmented ROIs are overlaid as colored regions on a structural MRI image. ROIs were further segmented according to left (ipsilateral) and right (contralateral) hemispheres, but are shown together here for clarity.

Author Manuscript Author Manuscript Author Manuscript Author Manuscript

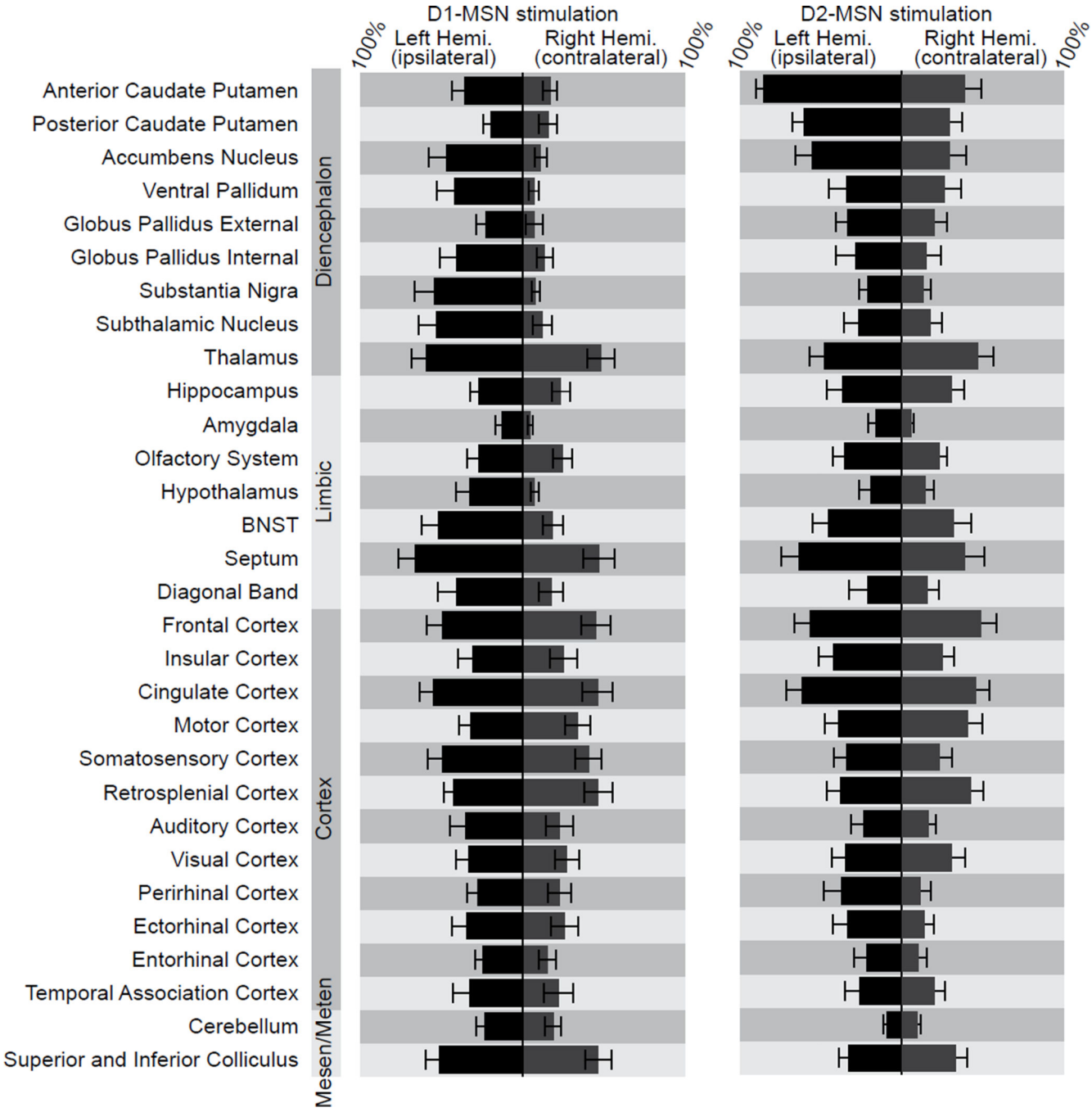

Figure 3. Whole-brain modulation volumes during D1- and D2-MSN stimulation measured with fMRI show robust activity in many regions across the brain

Values represent the percent of each ROI that is modulated by stimulation, and are shown as mean ± SEM across subjects (n = 12 D1-Cre and 11 D2-Cre mice). Regions are grouped according to subdivisions of standard developmental anatomical brain characterization (diencephalon, limbic system, cortex, mesencephalon, metencephalon).

Author Manuscript Author Manuscript Author Manuscript Author Manuscript

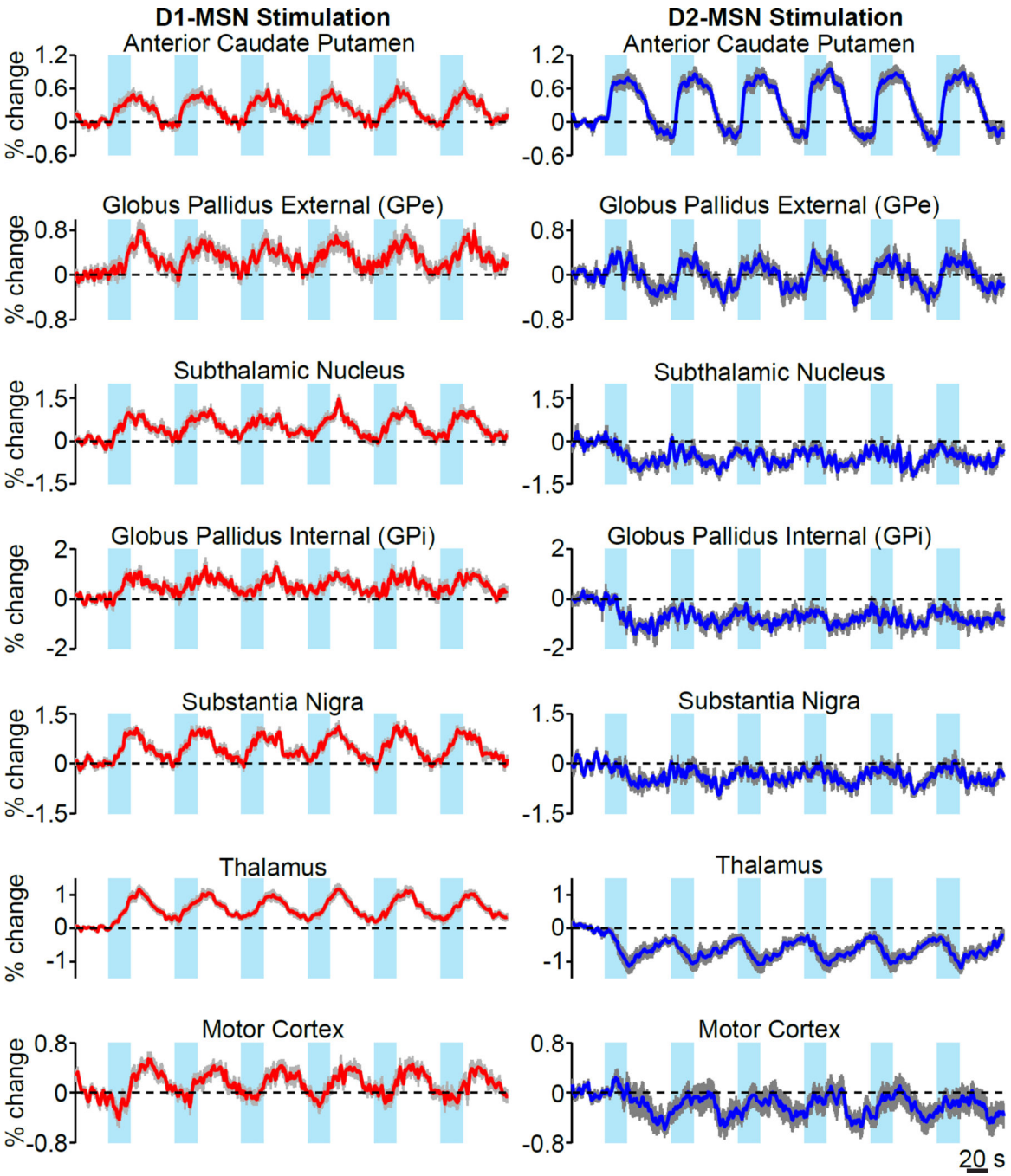

Figure 4. Functional MRI time series reveal differential effects of D1- and D2-MSN stimulation within the basal ganglia-thalamocortical loop

Average BOLD signal of active voxels in the ipsilateral basal ganglia-thalamocortical loop thresholded from n = 12 D1-Cre and 11 D2-Cre animals. Time series values are expressed as the percent signal change relative to a 30 s pre-stimulation baseline period. Values with errorbars are mean ± SEM See also Figure S2.

Author Manuscript Author Manuscript Author Manuscript Author Manuscript

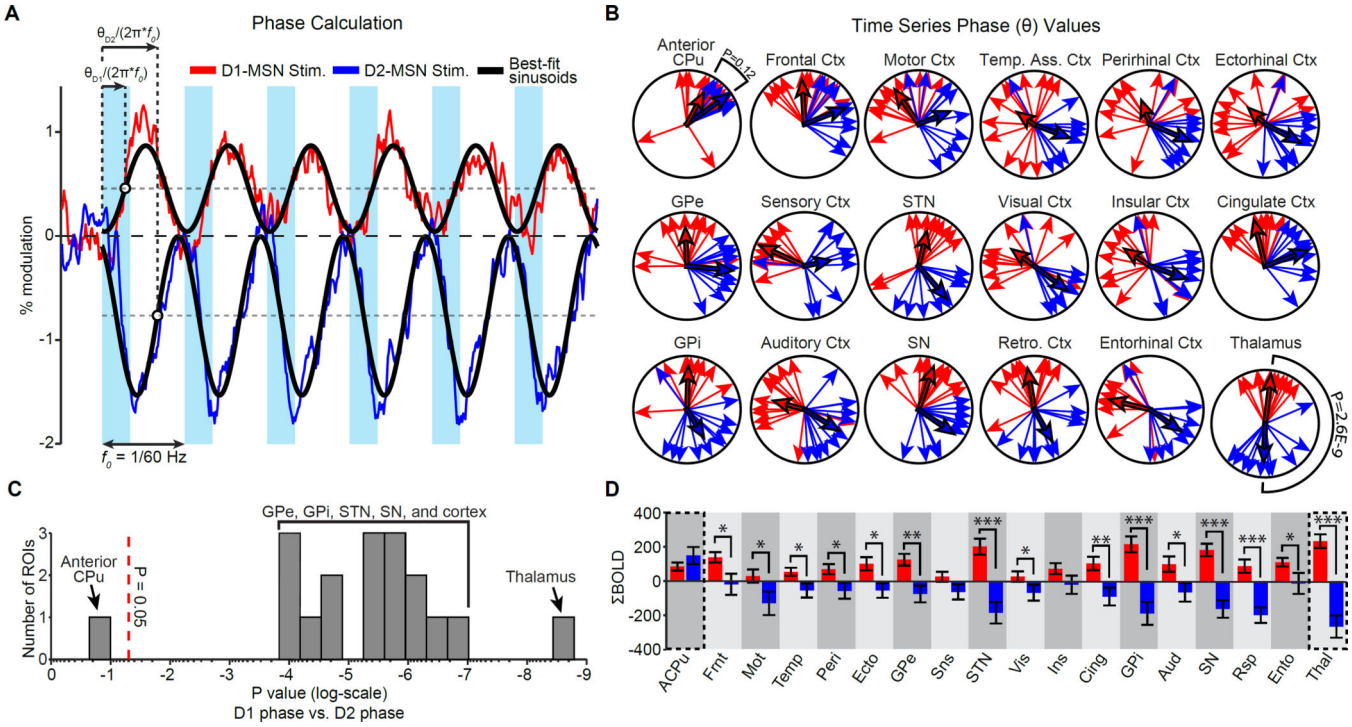

Figure 5. Stimulations of D1- and D2-MSNs drive distinct and opposing fMRI responses in the ipsilateral hemisphere

A, Schematic diagram of phase calculation for two fMRI time series. This example uses the average fMRI time series within the thalamus during D1- (red) and D2-MSN (blue) stimulation. Phase (θ) is calculated as the angle of the Fourier transform at the frequency of repeated stimulations (1/60 Hz). This corresponds to the temporal shift of the sinusoid that best fits the data in the least-squares sense (solid black lines). **B**, Distribution of phase values within the ipsilateral basal ganglia-thalamocortical loop during D1- and D2-MSN stimulation. Skinny arrows indicate subject-specific values. Bolded arrows indicate group averages. All regions, except the anterior caudate putamen (i.e. the site of stimulation), exhibit significantly different phase values between D1- and D2-MSN stimulation ($p < 0.001$, circular Watson-Williams test; $n = 12$ and 11 animals, respectively). Regions are sorted by p value in descending order from left to right. **C**, Histogram of p values from circular Watson-Williams tests in panel B. **D**, Quantification of ΣBOLD values for each ROI with statistical comparisons between D1- and D2-MSN stimulation (* $p < 0.05$, *** $p < 0.001$; two-tailed t-test). ΣBOLD was calculated as the summation of each ROI's average time series. See also Figures S3 and S4.

Author Manuscript Author Manuscript Author Manuscript Author Manuscript

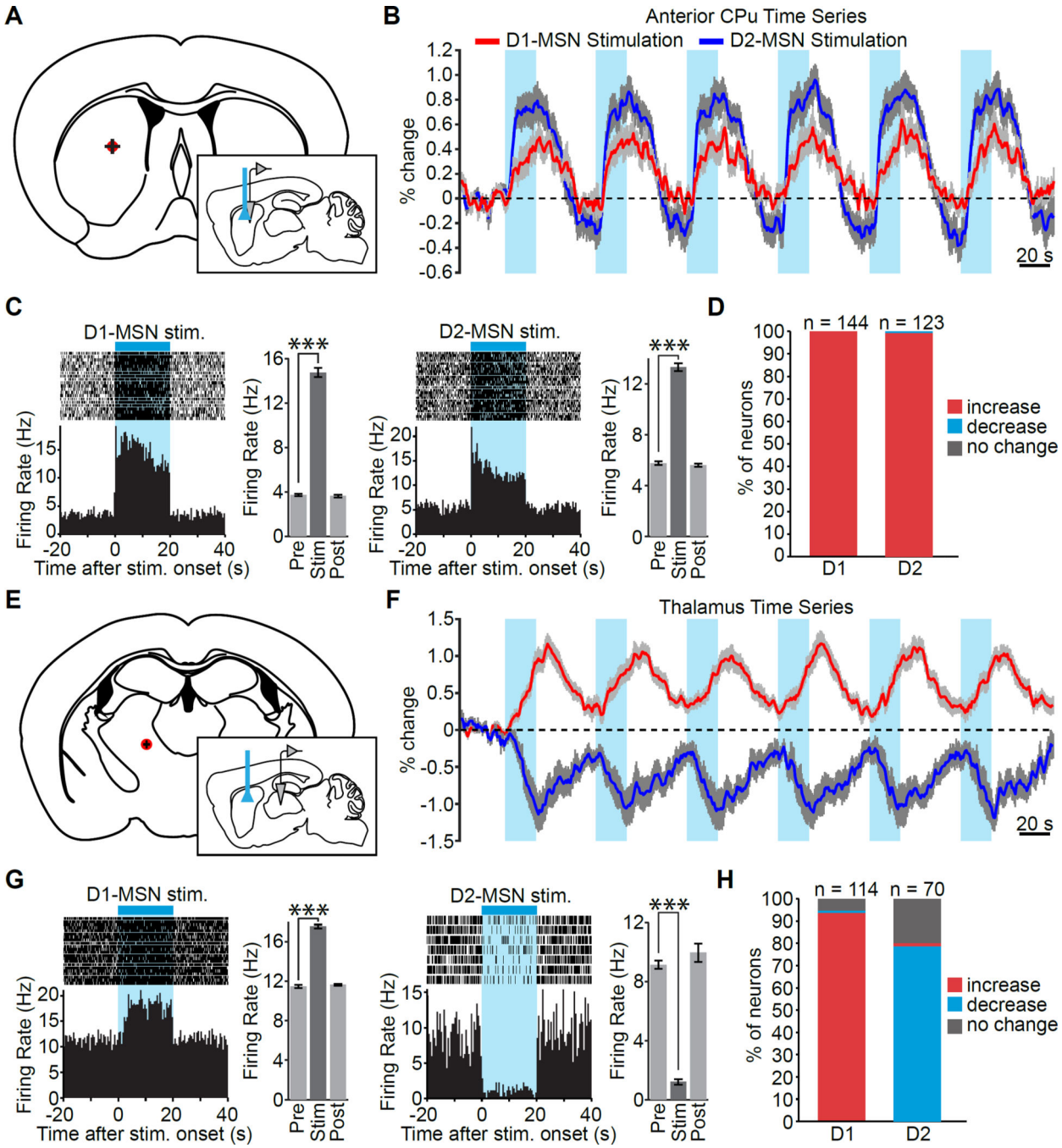

Figure 6. Neuronal activity mirrors the polarity of fMRI responses evoked in striatum and thalamus during D1- and D2-MSN stimulations

A,E, Schematics of single-unit recording locations within striatum and thalamus. Red dots indicate the average recording location, with crossbars indicating the standard deviation across animals. **B**, D1- and D2-MSN stimulations both drive robust, positive fMRI responses in striatum. Time series are averaged over all active voxels within the anterior caudate putamen ROI and are expressed as the percent signal change relative to a 30 s pre-stimulation baseline period. Values are presented as mean ± SEM across animals (n = 12 and

Author Manuscript Author Manuscript Author Manuscript Author Manuscript

11 for D1- and D2-MSN stimulation, respectively). **C**, Peri-event time histograms of two representative neurons illustrate the immediate and sustained increase in striatal neuronal activity during direct and indirect pathway stimulations. To the right of each histogram are the corresponding firing rates before, during, and after stimulation for that neuron (20 s periods, $n = 21$ and 26 trials, *** $P < 0.001$ one-tailed paired t-test, mean ± SEM). **D**, 100 and 99% of cells recorded in striatum during D1- and D2-MSN stimulation, respectively, exhibit an increase in firing rate. **F**, D1-MSN stimulation drives a robust positive BOLD response in thalamus, while D2-MSN stimulation drives a robust negative response. Analysis was the same as panel B. **G**, Peri-event time histograms of two representative neurons in thalamus during D1-and D2-MSN stimulation. Stimulation of the direct pathway evokes a sustained increase in neuronal activity, while stimulation of the indirect pathway evokes an immediate and sustained decrease in neuronal activity. To the right of each histogram are the corresponding firing rates before, during, and after stimulation for that neuron (20 s periods, $n = 22$ and 7 trials, *** $P < 0.001$ one-tailed paired t-test, mean ± SEM). **H**, 94% of cells recorded during D1-MSN stimulation exhibit an increase in firing rate, while 79% of recorded units during D2-MSN stimulation exhibit a decrease in firing rate. Changes in firing rate in panels D and H are determined by one-tailed paired t-tests.

Author Manuscript Author Manuscript Author Manuscript Author Manuscript

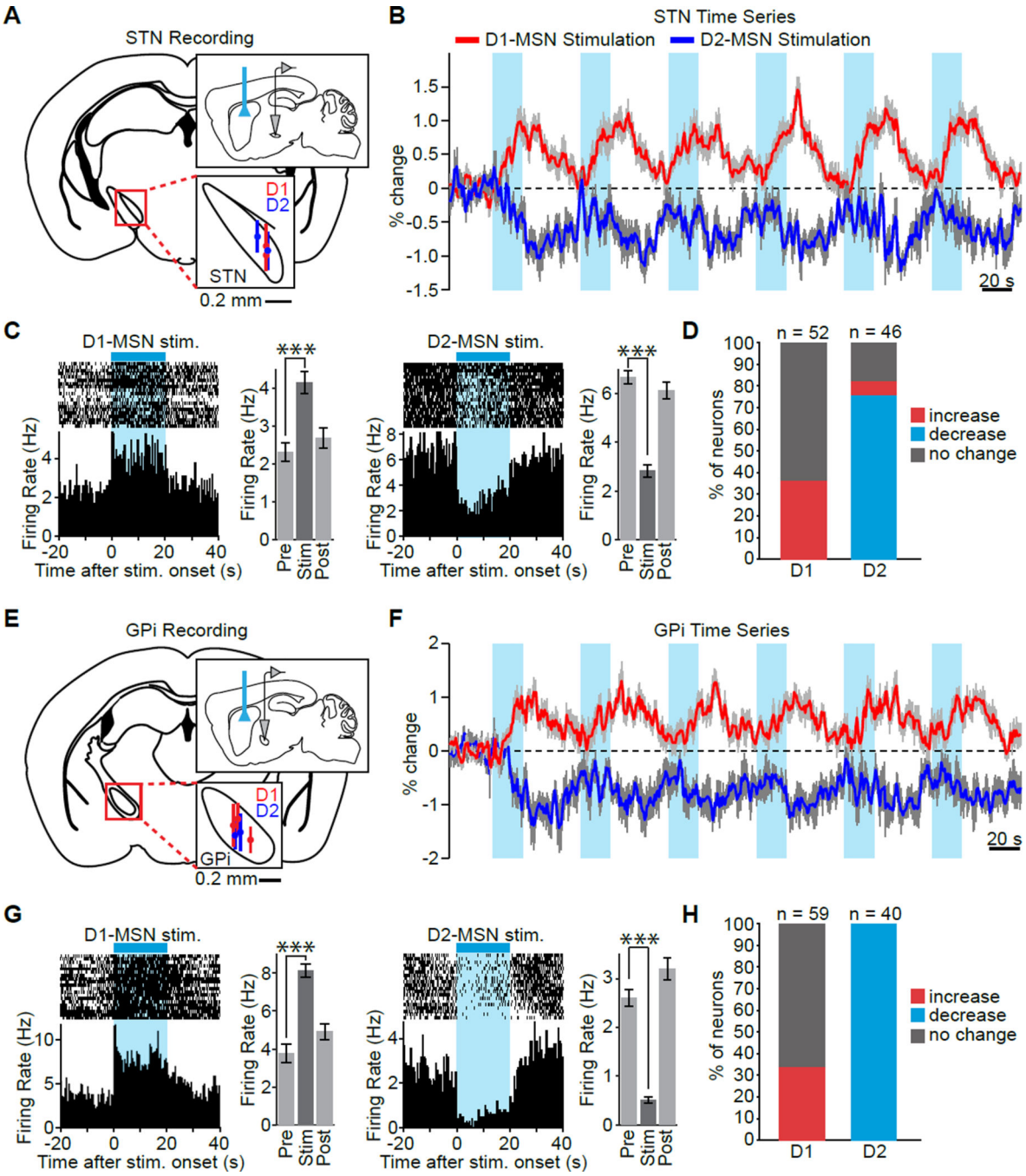

Figure 7. Neuronal activity mirrors the polarity of fMRI responses evoked in STN and GPi during D1- and D2-MSN stimulations

A,E, Schematics of single-unit recording locations within STN and GPi during striatal stimulation. Vertical lines within the magnified insets show the range of electrode contact placement for each animal. **B,F**, D1-MSN stimulation drives a robust positive BOLD response in STN and GPi, while D2-MSN stimulation drives a robust negative response in these two regions. Time series are averaged over all active voxels within each ROI and are expressed as the percent signal change relative to a 30 s pre-stimulation baseline period.

Author Manuscript Author Manuscript Author Manuscript Author Manuscript

Values are presented as mean ± SEM across animals (n = 12 and 11 for D1- and D2-MSN stimulation, respectively). **C,G**, Peri-event time histograms of representative STN and GPi neurons illustrate the increase in neuronal activity observed in these regions during direct pathway stimulation and the decrease in activity observed during indirect pathway stimulation. To the right of each histogram are the corresponding firing rates before, during, and after stimulation for that neuron (20 s periods, n = 20 trials, *** $P < 0.001$ one-tailed paired t-test, mean ± SEM). **D**, Quantification of single-unit response types in STN during D1- and D2-MSN stimulation. 37% of cells recorded in STN during D1-MSN stimulation (i.e. all modulated units) exhibit an increase in firing rate, while 76% of STN units exhibit a decrease in firing rate during D2-MSN stimulation. 7% of STN units also exhibit an increase in firing rate during D2-MSN stimulation. **H**, Quantification of single-unit response types in GPi during D1- and D2-MSN stimulation. 34% of cells recorded in GPi during D1-MSN stimulation (i.e. all modulated units) exhibit an increase in firing rate. 100% of GPi units exhibit a decrease in firing rate during D2-MSN stimulation.